DOI: https://doi.org/10.57233/ijsgs.v11i2.853

ISSNp: 2488-9229; ISSNe: 3027-1118

IJSGS FUGUSAU VOLXXX WEBSITE: https://fugus-ijsgs.com.ng

INTERNATIONAL JOURNAL OF SCIENCE FOR GLOBAL SUSTAINABILITY
(A PUBLICATION OF FACULTY OF SCIENCE, FEDERAL UNIVERSITY GUSAU, NIGERIA)

Effects of Heat Generation and Soret on Magnetohydrodynamic (MHD) Couette Flow with Radiation and Mass Absorption

Omokhuale E. and Dange M. S.

Department of Mathematical Sciences, Federal University Gusau, P. M. B. 1001, Zamfara State, Nigeria.

Corresponding Author's Email: emmanuelomokhuale@gmail.com

Received on: April, 2025 **Revised and Accepted on:** May, 2025 **Published on:** July, 2025

ABSTRACT

This article investigates the effects of heat generation and Soret on MHD Couette flow taking into consideration mass absorption and radiation influence. The governing flow in this study is modelled in the form of partial differential equations (PDEs) in dimensional form with initial and boundary conditions and the Couette fluid model is also be used to characterize the fluid behavior. Then, using suitable dimensionless quantities, the governing non-linear PDEs are transformed. Since the flow governing equations of the problem under investigation are highly complex and complicated, techniques that complement experimental and theoretical fluid dynamics by providing alternative potentially cheaper means of testing fluid flow systems is used. Therefore, the Finite Element Method (FEM) is used after discretization of the PDEs. Using graphs and tables, the effects of thermo physical parameters of engineering interests embedded in the velocity, temperature, concentration of the fluid were studied through series of numerical experiments and discussed. Furthermore, it is interesting to report that an excellent agreement was established when the results of this study was compared with those in literature, thereby authenticating and validating the accuracy of FEM as a strong tool. According to the results of this study, the actions of heat generation on the thermal and momentum boundary layers for increasing values are significant, also, increasing the Soret and thermal radiation cause a reverse trend i.e. decrease in the concentration, temperature and velocity of the fluid.

Keywords: MHD; Soret, Couette flow, thermal radiation, FEM.

1.0 INTRODUCTION

Magnetohydrodynamics (MHD) is a discipline of physics that discusses the properties of an electrically conducting fluid when it is exposed to a magnetic field. Numerous industrial applications can be found for these MHD principles, such as flow meters, generators, and MHD Pumps. MHD principle is well-exemplified by dynamo and motor. Many researchers are interested in MHD topics such as geophysics, Astrophysics, and plasma physics among others, and also find in biology and medicine (Goud & Reddy, 2022). Bafakeeh *et al.* (2022) studied unsteady MHD free convection heat and mass transfer flow of a viscous, incompressible, and electrically conducting fluid passing through a vertical plate embedded in a porous medium in the presence of chemical reactions and thermal radiation.

In Magnetohydrodynamic (MHD) Couette flow, the Soret effect, also known as thermal diffusion, plays a significant role in mass transfer due to temperature gradients. This effect is particularly important in situations where temperature differences cause the movement of different chemical species, leading to a separation of mass. Thus, Soret effect is referred to species differentiation developing in an initial homogeneous mixture submitted to a thermal gradient. Venkateswarlu *et al.* (2020) considered the effect of the fascinating and novel characteristics of Hall current and Soret number on hydromagnetic Couette flow in a rotating system with a convective boundary condition. Exact solutions for the fluid velocity, temperature, and species concentration, under Boussinesq approximation, are obtained in closed form by using the two-term perturbation technique. The interesting parts of thermal dispersing outcomes are taken into account. Sengupta & Ahmed (2017) presented analytically the parametric effect of thermo-diffusion (Soret) and diffusion-thermo (Dufour) effects on a two-dimensional steady magnetohydrodynamic (MHD) free convective heat and mass transfer flow of a reasonably viscous incompressible electrically conducting fluid in the presence of thermal radiation and zeroth-order heat generation (absorption) effects.

Further researches were conducted in this direction. Pandey & Kavitha (2025) examined Soret effect along with chemical reaction and radiation on flow of an electrically conductive, viscous fluid through a perpendicular plate, which is porous with oscillatory suction. The aim of this study is to investigate the effects of first-order temperature and chemical reaction and the transverse magnetic field characteristics. Sengupta (2015) reported two-dimensional steady laminar flow of a Newtonian electrically conducting incompressible

DOI: https://doi.org/10.57233/ijsgs.v11i2.853 ISSNp: 2488-9229; ISSNe: 3027-1118

viscous fluid past a permeable plate immersed in Darcian porous media in presence of thermal diffusion (Soret), thermal radiation, first order chemical reaction and heat generation/absorption effects. The exact solutions for velocity, temperature and concentration fields. Mat Noor *et al.* (2022) explored the time-dependent squeeze flow of magnetohydrodynamic Jeffrey fluid over permeable medium in the influences of Soret and Dufour, heat source/sink and chemical reaction. The presence of joule heating, joule dissipation and radiative heat transfer are analyzed.

More so, Couette flow in fluid dynamics is known as laminar flow of a viscous fluid in the space between the two parallel plates, one of which moves relative to the other. This flow is driven by virtue of viscous drag force acting on fluid and the applied pressure gradient is parallel to the plate. This flow was named after Maurice Marie Alfred Couette in the 19th Century. The Couette flow of non-Newtonian fluids has got significant industrial applications such as preservation and processing of food products in food industries, chemical processing, power engineering, and petroleum production industries so on. In the recent past, several studies were carried out in the field of non-Newtonian fluids, especially in the field of biomedical and bioengineering applications. The heat transfer process occurs in three ways in fluids, i.e., the temperature differences in the particles which can be due to convection, conduction, and radiation (Uma *et al.*, 2019). Kabir *et al.* (2023) revealed the impact of suction/injection and permeability of porous materials on a steady natural convection Couette flow of a viscous incompressible fluid passing through a vertical porous plate. Mishra & Panda (2022) studied the consequence of viscous dissipation and Soret effects on hydromagnetic mixed convection flow across a porous medium bounded by infinite vertical plates. The flow considered is fully developed time-dependent. Viscous dissipation causes variations in fluid temperature and fluid properties. Ahmed *et al.* (2020) investigated the mechanism of both positive and negative effects of Soret-Dufour with heat and mass transfer processes over an accelerating permeable surface. The partial differential flow equations were simplified using similarity variables, and the resulting equations were solved numerically using the spectral homotopy analysis method (SHAM).

Consequently, thermal radiation is the transfer of heat in the form of electromagnetic waves, primarily in the infrared spectrum, emitted by objects due to their temperature. In engineering and scientific applications, understanding thermal radiation is essential for optimizing heat transfer processes, especially in high-temperature environments where conventional conduction or convection alone is insufficient. Thermal radiation plays a critical role in systems such as solar energy collectors, heat exchangers, and cooling mechanisms for electronics, where effective thermal management enhances performance and efficiency (Pasha *et al*., 2025).

Finite Element Method (FEM) is a numerical technique used to obtain an approximate solution to boundary value problems as they consist of elliptic partial differential equations and the boundary conditions. It has been applied to many physical problems. Omokhuale et al. (2019) examined unsteady heat and mass transfer magnetohydrodynamic (MHD) convective Couette flow with thermal radiation using Finite Element Method (FEM). Omokhuale and Jabaka (2022a) researched on the effect of heat source on unsteady hydromagnetic convective Couette flow of a viscous, electrically conducting and incompressible fluid is investigated. The effects of heat sink and radiation on unsteady hydromagnetic convective Couette flow of a viscous electrically conducting and incompressible fluid was studied by Omokhuale and Jabaka (2022b). The governing equations that describe the flow formation, heat and mass transfer are modeled as Partial Differential Equations (PDEs) and solved numerically using Finite FEM.

This research attempts to extend the work of Omokhuale and Jabaka (2022b) by incorporating the effects of thermal radiation, magnetic field and mass absorption parameters using FEM. With the help of line graphs, the deviations of different impacting parameters are thoroughly examined.

2.0 PROBLEM FORMULATION

Imagine MHD Couette flow of an electrically conducting fluid in a channel. The assumptions stated below were considered: (i) The x^*-axis and y^*- axis is taken along the plate in the vertical upward and normal direction to the plate respectively. (ii) The transverse magnetic field of uniform strength B_o is applied normal to the plate. (iii) The fluid has thermal radiation, Soret, heat generation and mass absorption. The Boussinesq's approximation is taken for the flow.

Premised on these assumptions, the unsteady flow is governed by the following partial differential equations viz: continuity, momentum, energy and mass equations.

DOI: https://doi.org/10.57233/ijsgs.v11i2.853 ISSNp: 2488-9229; ISSNe: 3027-1118
IJSGS FUGUSAU VOLXXX WEBSITE: https://fugus-ijsgs.com.ng

$$\frac{\partial v^*}{\partial y^*} = 0 \tag{1}$$

$$\frac{\partial u^*}{\partial t^*} = v\frac{\partial^2 u^*}{\partial y^{*2}} + g\beta_1\left(T^* - T_h^*\right) + g\beta_2\left(C^* - C_h^*\right) - \frac{\sigma\mu_e^2 B_0^2}{\rho}\left(u^* - U_0 t^{*n}\right) \tag{2}$$

$$\frac{\partial T^*}{\partial t^*} = \frac{k}{\rho Cp}\frac{\partial^2 T^*}{\partial y^{*2}} - \frac{1}{\rho Cp}\frac{\partial q_r}{\partial y^*} + \frac{Q_T}{\rho Cp}\left(T^* - T_h^*\right) + Q_m\left(C^* - C_h^*\right) \tag{3}$$

$$\frac{\partial C^*}{\partial t^*} = D\frac{\partial^2 C^*}{\partial y^{*2}} - R_m^*\left(C^* - C_h^*\right) + \frac{D_m K_T}{T_m}\frac{\partial^2 T^*}{\partial y^{*2}} \tag{4}$$

The corresponding initial and boundary conditions are:

$$\left.\begin{aligned} t^* \le 0 &: u^* = 0, T^* = T_h^*, C^* = C_h^* \quad for \quad 0 \le y^* \le h \\ t^* > 0 &: \begin{cases} u^* = U_0, T^* = T_h^*, C^* = C_h^* & at\ y^* = 0 \\ u^* = 0, T^* = T_h^*, C^* = C_h^* & at\ \ y^* = h \end{cases} \end{aligned}\right\} \tag{5}$$

Applying the Rosseland approximation, the radiative heat flux q_r is defined as:

$$q_r = -\frac{4\sigma^*}{3k}\frac{\partial T^{*4}}{\partial y^*}$$

we assume that the difference in temperature within the flow are sufficiently small such that q_r may be presented as a linear function of T^*. Therefore, on expanding T^{*4} in Taylor series about T_b^* up to first order approximation will give

$$T^{*4} = T_h^* + 4\left(T^* - T_h^*\right)T_h^{*3} = 4T^*T_h^{*3} - 3T_h^{*4} \tag{6}$$

Using Equations (5) and (6) in the last term of Equation (2), we got:

$$\frac{\partial q_r}{\partial y^*} = -\frac{16\sigma T_b^{*3}}{3k}\frac{\partial^2 T^*}{\partial y^{*2}} \tag{7}$$

Introducing Equation (7) into Equation (2), the heat equation becomes:

$$\frac{\partial T^*}{\partial t^*} = \frac{k}{\rho Cp}\frac{\partial^2 T^*}{\partial y^{*2}} + \frac{16\sigma T_h^{*3}}{3k^*\rho Cp}\frac{\partial^2 T^*}{\partial y^{*2}} + \frac{Q_c}{\rho Cp}\left(T^* - T_h^*\right) + \frac{Q_m}{\rho Cp}\left(C^* - C_h^*\right) \tag{8}$$

We will Introducing the following dimensionless quantities in Equations (2), (3) and (4):

$$\left.U = \frac{u^*}{h}, Y = \frac{y^*}{h}, t = \frac{t^*\nu}{h^2}, \phi = \frac{T^* - T_h^*}{T_w^* - T_h^*}, \varphi = \frac{C^* - C_h^*}{C_w^* - C_h^*},\right\} \tag{9}$$

The dimensionless form of Equations (1), (3) and (8) when the dimensionless quantities in equation (9) is used are:

$$\frac{\partial^2 U}{\partial y^2} - \frac{\partial U}{\partial t} + Gr\phi + Gc\varphi - M^2\left(U - Ft^n\right) = 0 \tag{10}$$

$$\frac{1}{\Pr}\left(1 + \frac{3}{4}R\right)\frac{\partial^2 \phi}{\partial y^2} - \frac{\partial \phi}{\partial t} + S\phi + \lambda\varphi = 0 \tag{11}$$

$$\frac{1}{Sc}\frac{\partial^2 \varphi}{\partial y^2} - \frac{\partial \varphi}{\partial t} + R_m\varphi - \gamma\frac{\partial^2 \phi}{\partial y^2} = 0 \tag{12}$$

DOI: https://doi.org/10.57233/ijsgs.v11i2.853 ISSNp: 2488-9229; ISSNe: 3027-1118
IJSGS FUGUSAU VOLXXX WEBSITE: https://fugus-ijsgs.com.ng

initial and boundary conditions (4) in dimensionless forms are:

$$\left.\begin{aligned} t \le 0 &: U = 0, \phi = 0, \varphi = 0 \quad for \quad 0 \le y \le h \\ t > 0 &: \begin{cases} U = F, \phi = 1, \varphi = 1 \quad at\ y = 0 \\ U = 0, \phi = 0, \varphi = 0 \quad at\ \ y = h \end{cases} \end{aligned}\right\} \tag{13}$$

Two cases are investigated, to obtain the solutions of Equations (10) to (12) subject to the initial and boundary conditions (13):

1. Impulsive movement of the plate at $y = 0$ (i.e., $n = 0$) and
2. Uniform accelerated movement of the plate at $y = 0$ (i.e., $n = 1$).

Case (1): Impulsive movement of the plate at $y = 0$:

Taking $n = 0$ in Equation (10), then the Equation (10) can be expressed as

$$\frac{\partial^2 U}{\partial y^2} - \frac{\partial U}{\partial t} + Gr\phi + Gc\varphi - M^2\left(U - F\right) = 0 \tag{14}$$

and the corresponding boundary conditions (13) reduce to

$$\left.\begin{aligned} t \le 0 &: U = 0, \phi = 0, \varphi = 0 \quad for \quad 0 \le Y \le h \\ t > 0 &: \begin{cases} U = F, \phi = 1, \varphi = 1 \quad at\, Y = 0 \\ U = 0, \phi = 0, \varphi = 0 \quad at\ \ Y = h \end{cases} \end{aligned}\right\} \tag{15}$$

2. Case (2): Uniform accelerated movement of the plate at $y = 0$.

Taking $n = 1$ in Equation (10), then the Equation (10) can be written as

$$\frac{\partial^2 U}{\partial y^2} - \frac{\partial U}{\partial t} + Gr\phi + Gc\varphi - M^2\left(U - Ft\right) = 0 \tag{16}$$

and the initial and boundary conditions (13) reduce to

$$\left.\begin{aligned} t \le 0 &: U = 0, \phi = 0, \varphi = 0 \quad for \quad 0 \le Y \le h \\ t > 0 &: \begin{cases} U = 0, \phi = 1, \varphi = 1 \quad at\, Y = 0 \\ U = 0, \phi = 0, \varphi = 0 \quad at\ \ Y = h \end{cases} \end{aligned}\right\} \tag{17}$$

For practical engineering applications and the design of chemical engineering systems, quantities of interest viz. Skin-friction, Nusselt and Sherwood numbers which are necessary to compute. The skin-friction or the shear tress at the moving plate of the channel in dimensionless form is given by

$$\tau = -\left(\frac{\tau_w^*}{\rho u_0 \nu}\right)_{y^*=0} = -\left(\frac{\partial U}{\partial y}\right)_{y^*=0} \tag{18}$$

The rate of heat transfer at the moving hot plate of the channel in dimensionless form is illustrated by

$$Nu_0 = -x^* \frac{\left(\frac{\partial \phi^*}{\partial y^*}\right)_{y^*=0}}{\phi_w^* - \phi_b^*} \Rightarrow Nu_0\, \mathrm{Re}_x^{-1} = -\left(\frac{\partial \phi}{\partial Y}\right)_{Y=0} \tag{19}$$

Also, the rate of heat transfer on the stationary plate is given by

$$Nu_1 = -x^* \frac{\left(\frac{\partial \phi^*}{\partial y^*}\right)_{y^*=b}}{\phi_w^* - \phi_b^*} \Rightarrow Nu_1\, \mathrm{Re}_x^{-1} = -\left(\frac{\partial \phi}{\partial Y}\right)_{Y=1} \tag{20}$$

The Sherwood number at the moving plate of the channel in dimensionless form is given by

DOI: https://doi.org/10.57233/ijsgs.v11i2.853 ISSNp: 2488-9229; ISSNe: 3027-1118
IJSGS FUGUSAU VOLXXX WEBSITE: https://fugus-ijsgs.com.ng

$$Sh = -x^* \frac{\left(\frac{\partial \varphi^*}{\partial y^*}\right)_{y^*=0}}{\varphi_w^* - \varphi_b^*} \Rightarrow Sh\,\mathrm{Re}_x^{-1} = -\left(\frac{\partial \varphi}{\partial Y}\right)_{Y=0} \quad (21)$$

where Re_x is the Reynold's number. The mathematical modeling of the problem is now done. So, equations (11), (12), (14) and (16) presents a coupled system of linear PDEs and these are to be solved with initial and boundary conditions (15) and (17). Therefore, finding the exact solutions are complicated, whenever it is possible. Thus, these equations are solved numerically by FEM.

3.0 Numerical Solutions by FEM

The FEM is an efficient numerical and computational method to solving a variety of engineering and real-world problems. So many developers, researchers and users have recognized this method as one of the most powerful numerical analysis tools useful to analyze complex engineering problems. The simplicity, flexibility, computability and accuracy of the method make it significant in modeling and design process. This is because of the discretization of domain of the problem is done employing highly flexible elements or uniform or non-uniform patches that can be easily shown as complex shapes. The method vitally comprises the piecewise continuous functions in a systematic way that reduces the error in the solution.

The procedures involved in the finite element analysis as follows:
procedure 1: Discretization of the domain
procedure 2: Generation of the element equations
procedure 3: Assembling of the element equations
procedure 4: Imposition of the boundary conditions
procedure 5: Solution of assembled equations
Variational Formulation

The Variational formulation associated with Equations (10) to (12) over a typical two-noded linear element (y_e, y_{e+1}) is given by

$$\int_{y_e}^{y_{e+1}} z_1 \left[\left(\frac{\partial U}{\partial t}\right) - \left(\frac{\partial^2 U}{\partial y^2}\right) - Gr(\phi) - Gc(\varphi) + M^2\left(U - Ft^n\right)\right] dy = 0 \quad (22)$$

$$\int_{y_e}^{y_{e+1}} z_2 \left[\left(\frac{\partial \phi}{\partial t}\right) - \frac{1}{\mathrm{Pr}}\left(1 + \frac{3}{4}R\right)\left(\frac{\partial^2 \phi}{\partial y^2}\right) + S(\phi) + \lambda\varphi\right] dy = 0 \quad (23)$$

$$\int_{y_e}^{y_{e+1}} z_3 \left[\left(\frac{\partial \varphi}{\partial t}\right) - \frac{1}{Sc}\left(\frac{\partial^2 \varphi}{\partial y^2}\right) - R_m(\varphi) + \gamma\left(\frac{\partial^2 \phi}{\partial y^2}\right)\right] dy = 0 \quad (24)$$

where z_1, z_2 and z_3 are arbitrary test functions and may be seen as the variation in u, T and C respectively. When the order of integration was reduced, we got the following system of equation:

$$\int_{y_e}^{y_{e+1}} z_1 \left[z_1\left(\frac{\partial u}{\partial t}\right) + \left(\frac{\partial z_1}{\partial y^2}\right)\left(\frac{\partial U}{\partial y}\right) + \left(M^2\right)(z_1)U - (F)(z_1)t^n - (Gr)(z_1)\phi - (Gc)(z_1)\varphi\right] dy$$
$$- \left[(z_1)\left(\frac{\partial U}{\partial y}\right)\right]_{y_e}^{y_{e+1}} = 0 \quad (25)$$

$$\int_{y_e}^{y_{e+1}} \left[(z_2)\left(\frac{\partial \phi}{\partial t}\right) - \frac{1}{\mathrm{Pr}}\left(1 + \frac{3}{4}R\right)\left(\frac{\partial z_2}{\partial y}\right)\left(\frac{\partial \phi}{\partial y}\right) - (S)(z_2)(\phi)\right] dy - \left[\left(\frac{z_2}{\mathrm{Pr}}\right)\left(\frac{\partial \phi}{\partial y}\right)\right]_{y_e}^{y_{e+1}} = 0 \quad (26)$$

DOI: https://doi.org/10.57233/ijsgs.v11i2.853 ISSNp: 2488-9229; ISSNe: 3027-1118

IJSGS FUGUSAU VOLXXX WEBSITE: https://fugus-ijsgs.com.ng

$$\int_{y_e}^{y_{e+1}}\left[(z_3)\left(\frac{\partial\varphi}{\partial t}\right)+\frac{1}{Sc}\left(\frac{\partial z_3}{\partial y}\right)\left(\frac{\partial\varphi}{\partial y}\right)-(R_m)(z_3)(\varphi)-\gamma(z_3)(\phi)\right]dy-\left[\left(\frac{z_3}{Sc}\right)\left(\frac{\partial\varphi}{\partial y}\right)\right]_{y_e}^{y_{e+1}}=0 \quad (27)$$

3.1 Finite Element Formulation:

The finite element model can be gotten from Equations (25) to (27) by substituting the finite element approximations of the form:

$$U=\sum_{k=1}^{2}U_k^e\xi_k^e,\phi=\sum_{k=1}^{2}\phi_k^e\xi_k^e \text{ and } \sum_{k=1}^{2}\varphi_k^e\xi_k^e \quad (28)$$

with $z_1=z_2=z_3=\xi_k^e\,(k=1,2)$, U_k^e,ϕ_k^e and φ_k^e are the velocity, temperature and concentration respectively at the k^{th} node of typical e^{th} element (y_e,y_{e+1}) and ξ_k^e are the shape functions for this element (Y_e,Y_{e+1}) and are taken as:

$$\xi_1^e=\frac{y_{e+1}-y}{y_{e+1}-y_e} \text{ and } \xi_2^e=\frac{y-y_e}{y_{e+1}-y_e},\ y_e\le y\le y_{e+1} \quad (29)$$

This finite element model of the equations for

$$\begin{bmatrix}[P^{11}] & [P^{12}] & [P^{13}]\\ [P^{21}] & [P^{22}] & [P^{23}]\\ [P^{31}] & [P^{32}] & [P^{33}]\end{bmatrix}\begin{bmatrix}\{U^e\}\\ \{\phi^e\}\\ \{C^e\}\end{bmatrix}+\begin{bmatrix}[W^{11}] & [W^{12}] & [W^{13}]\\ [W^{21}] & [W^{22}] & [W^{23}]\\ [W^{31}] & [W^{32}] & [W^{33}]\end{bmatrix}\begin{bmatrix}\{U'^e\}\\ \{\phi'^e\}\\ \{\varphi'^e\}\end{bmatrix}=\begin{bmatrix}\{a^{1e}\}\\ \{a^{2e}\}\\ \{a^{3e}\}\end{bmatrix} \quad (30)$$

where $\{\{P^{mn}\},\{W^{mn}\}\}$ and $\{\{U^e\},\{\phi^e\},\{\varphi^e\},\{U^e\},\{\phi^e\},\{\varphi^e\},\{a^{me}\}\}\,(m=1,2,3)$ are the set of matrices of order 2×2 and 2×1 respectively and $'$ (dash) indicates $\frac{d}{dy}$.

These matrices are defined as follows:

$$P_{Ik}^{11}=\int_{y_e}^{y_{e+1}}\left[\left(\frac{\partial\xi_i^e}{\partial y}\right)\left(\frac{\partial\xi_k^e}{\partial y}\right)\right]dy+(M^2)\int_{y_e}^{ye+1}\left[(\xi_i^e)(\xi_k^e)\right]dy-Ft^n\int_{y_e}^{ye+1}(\xi_i^e)dy,$$

$$P_{ik}^{12}=-Gr\int_{y_e}^{ye+1}\left[(\xi_i^e)(\xi_k^e)\right]dy,P_{ik}^{13}=-Gc\int_{y_e}^{ye+1}\left[(\xi_i^e)(\xi_k^e)\right]dy,W_{ik}^{11}=\int_{y_e}^{ye+1}\left[(\xi_i^e)(\xi_k^e)\right]dy,W_{ik}^{12}=W_{ik}^{13}=0,$$

$$W_{ik}^{21},W_{ik}^{23}=0,W_{ik}^{31}=W_{ik}^{32}=0,P_{ik}^{21}=0,P_{ik}^{31}=0,b_i^{1e}=\left[(\xi_i^e)\left(\frac{\partial u}{\partial y}\right)\right]_{y_e}^{y_{e+1}}$$

$$P_{ik}^{22}=\frac{1}{\Pr}\left(\frac{3R+4}{3R}\right)\int_{y_e}^{ye+1}\left[\left(\frac{\partial\xi_i^e}{\partial y}\right)\left(\frac{\partial\xi_k^e}{\partial y}\right)\right]dy,P_{ik}^{23}=-S\int_{y_e}^{ye+1}\left[(\xi_i^e)(\xi_k^e)\right]dy,$$

DOI: https://doi.org/10.57233/ijsgs.v11i2.853 ISSNp: 2488-9229; ISSNe: 3027-1118

IJSGS FUGUSAU VOLXXX WEBSITE: https://fugus-ijsgs.com.ng

$$P_{ik}^{33} = \frac{1}{Sc}\int_{Y_e}^{Ye+1}\left[\left(\frac{\partial \xi_i^e}{\partial Y}\right)\left(\frac{\partial \xi_k^e}{\partial Y}\right)\right]dy,$$

$$W_{ik}^{22}\int_{y_e}^{ye+1}\left[\left(\xi_i^e\right)\left(\xi_k^e\right)\right]dy, P^{25} = R_m\int_{y_e}^{ye+1}\left[\left(\xi_i^e\right)\left(\xi_k^e\right)\right]dy, P^{26} = \gamma\int_{y_e}^{ye+1}\left[\left(\xi_i^e\right)\left(\xi_k^e\right)\right]dy$$

$$a_i^{2e} = \left[\left(\frac{\xi_i^e}{\Pr}\right)\left(1+\frac{3}{4}R\right)\left(\frac{\partial \phi}{\partial Y}\right)+S\left(\xi_i^e\right)\right]_{y_e}^{y_{e+1}},\ a_i^{3e} = \left[\left(\frac{\xi_i^e}{Sc}\right)\left(\frac{\partial \varphi}{\partial y}\right)\right]_{y_e}^{y_{e+1}} \text{ and } W_{ik}^{33} = \int_{y_e}^{ye+1}\left[\left(\xi_i^e\right)\left(\xi_k^e\right)\right]dy.$$

In one-dimensional space, linear element, quadratic element or element of higher order can be used. The entire flow domain is divided into 10,000 quadratic elements of equal size. Each element is three-noded, and as such the whole domain contains 20,001 nodes. At each node, three functions are to be evaluated: hence, after assembling of the element equations, we got a system of 80,004 equations which are linear. Thus, an iterative scheme must be employed in the solution. On imposing the boundary conditions, a system of equations was gotten which is solved by Gauss elimination method while maintaining an accuracy of 0.00001. A convergence criterion based on the relative difference between the current and previous iterations is used. After these differences satisfy the desired accuracy, the solution is assumed to have been converged and iterative process terminated. The Gaussian quadrature is implemented for solving the integrations. The code of the algorithm has been executed twice in MAPLE for cases 1 and 2. Excellent results was seen for all results.

3.2 Study of Grid Independence

In general, to study the grid independency/dependency, the mesh size is varied in order to check the solution at different mesh (grid) sizes and get a range at which there is no variation in the solutions.

4.0 DISCUSSION OF RESULTS

The effects of heat generation and Soret on MHD Couette flow in the presence thermal radiation and mass absorption were studied. Furthermore, a Maple program is written to generate line graphs for the velocity, temperature and concentration profiles in other to provide a clear insights of the problem at hand where the effects of major controlling factors such as: Soret γ, heat generation parameter S, magnetic field effect M, thermal radiation parameter (R), thermal Grashof number (Gr), mass Grashof number (Gc), heat sink parameter (R), chemical reaction parameter (Rc), Prandit number (Pr), Schmidt number (Sc). The default values selected for this present analysis are: $Pr = 0.71, Sc = 0.30, R = Rc = S = M = Gc = Gr = \gamma = 1$. The results obtained by Omokhuale and Jabaka (2022b) was compared with this current investigation. The comparison confirms an excellent agreement.

Figures 1 and 2 depict the effects of thermal and mass Grashof numbers on the velocity profiles. It is found that, there is significance in the velocity due to the enhancement of thermal buoyancy force. Also, the peak value of the velocity increases rapidly near the porous plate and the decays smoothly for free steam velocity. It is further noticed that the fluid velocity increases and the peak value is more distinctive due to increase in species buoyancy force. Thus, the velocity distribution attains a distinctive maximum value in the vicinity of the plate and then reduces properly to approach free stream value. The effect of Hartman number on the velocity profiles is as illustrated in Figure 3. It is observed that, the velocity of the fluid falls with increasing Hartman number. This is due to the Lorentz force, which is present when a magnetic field is applied to an electrically conductive fluid and a resistance force is produced. This force causes the fluid flow to slow down as it approaches the plate. As a result, all other forces, including the Lorentz force, vanish when the fluid comes to rest. Figure 4 shows the effect of Prandtl number on the velocity profiles. In Figure 5, the effect of Schmidt number is displayed. The effect of heat generation parameter on the velocity of the fluid is plotted in Figure 6. Figure 7 shows the effect of Soret number on the velocity profiles. Figure 8 illustrates the effect of Pr number on the temperature profiles. From this Figure, it is depicted that the temperature becomes lower as Prandtl number is increased. The effect of heat generation on the velocity profiles in the thermal boundary layer is provided in Figure 9. It is viewed that, increase in the heat generation parameter leads in rise of the momentum boundary layer of the fluid. Figure 10 shows the effect of thermal radiation on the temperature of the fluid. It is viewed that increasing values of thermal radiation parameter causes the fluid temperature to rise. In Figure 11, the effect of mass absorption on the temperature of the fluid is presented.

Figures 12 and 13 provide the concentration field because of variation in Schmidt number and Soret number respectively. It is understood that; the concentration of the

DOI: https://doi.org/10.57233/ijsgs.v11i2.853 ISSNp: 2488-9229; ISSNe: 3027-1118

fluid falls as the Schmidt number is increased and a similar trend is seen as chemical reaction rises. Physically, this occurs because increase in Sc means decrease of molecular diffusivity, which results in decrease of concentration boundary layer. Hence, the concentration of species is smaller for higher values of Sc.

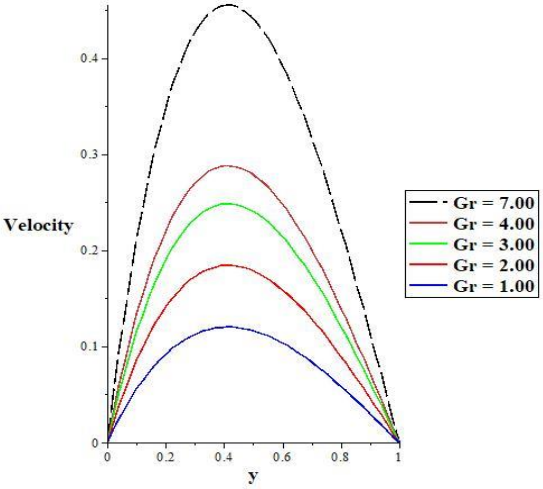

Figure 1: Effect of *Gr* on the velocity.

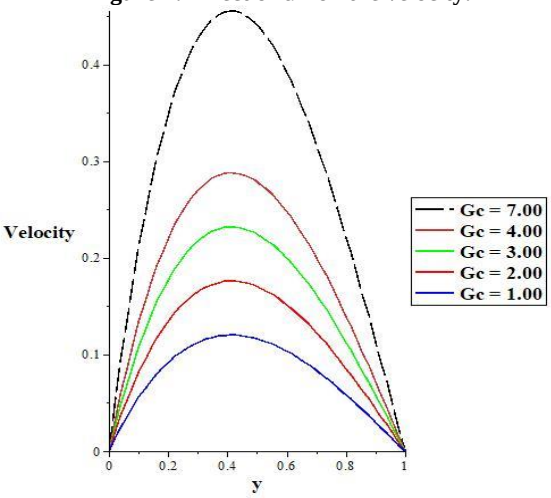

Figure 2: Effect of *Gc* on the velocity.

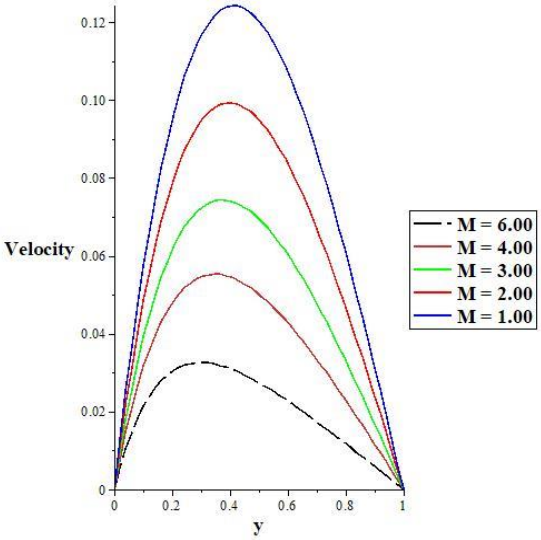

Figure 3: Effect of *M* on the velocity.

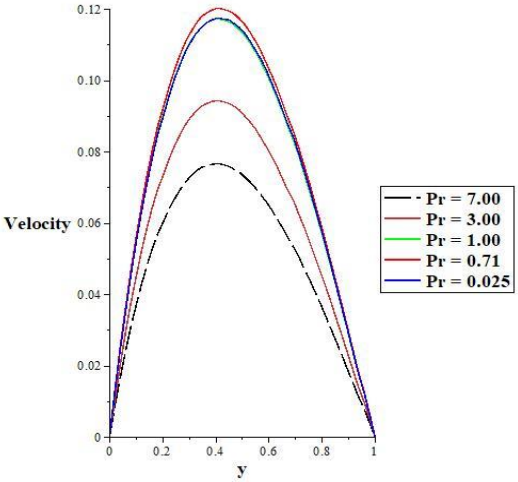

Figure 4: Effect of *Pr* on the velocity.

DOI: https://doi.org/10.57233/ijsgs.v11i2.853 ISSNp: 2488-9229; ISSNe: 3027-1118

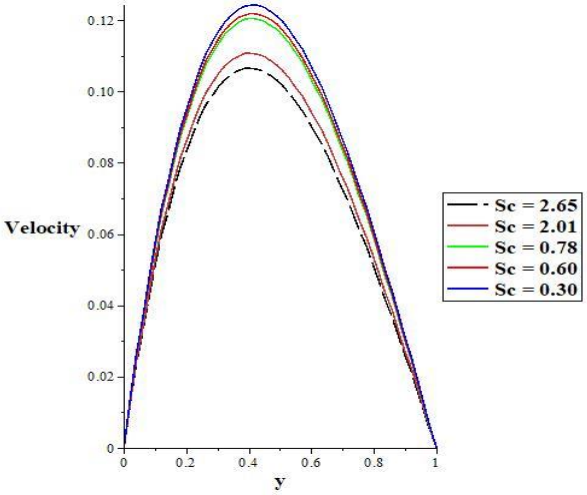

Figure 5: Effect of *Sc* on the velocity.

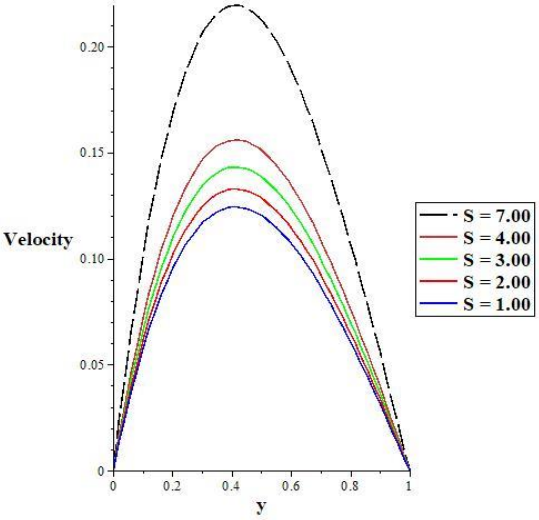

Figure 6: Effect of *S* on the velocity.

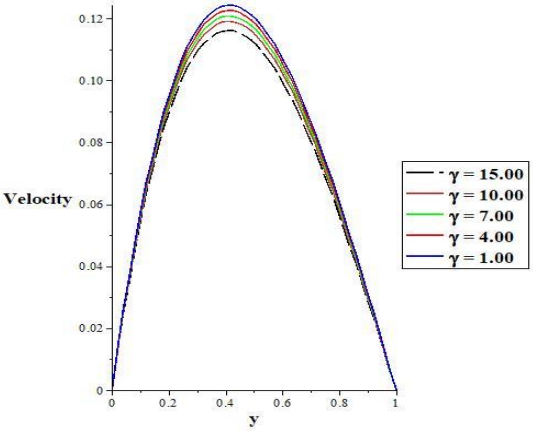

Figure 7: Effect of γ on the velocity.

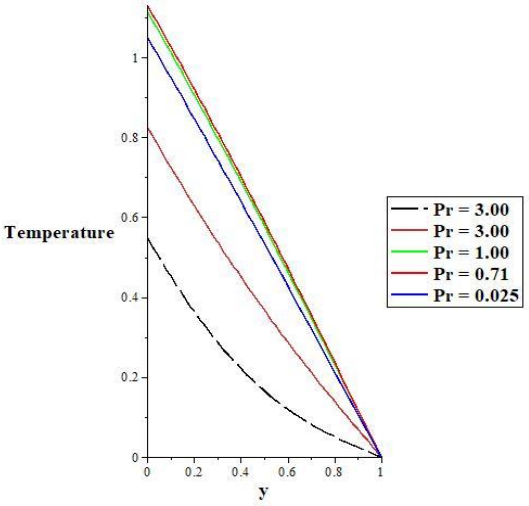

Figure 8: Effect of *Pr* on the temperature.

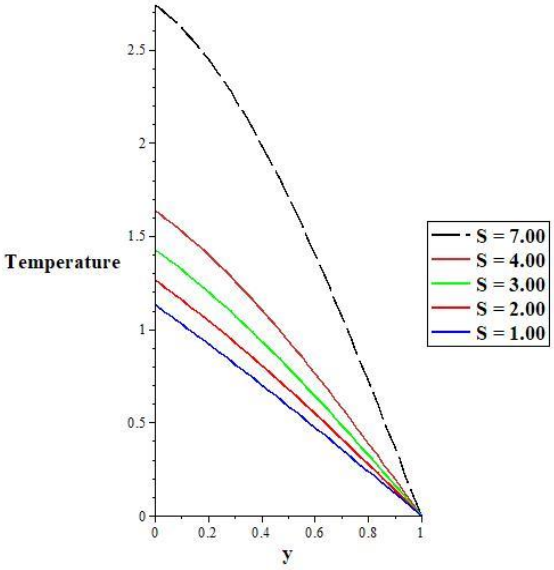

Figure 9: Effect of *S* on the temperature.

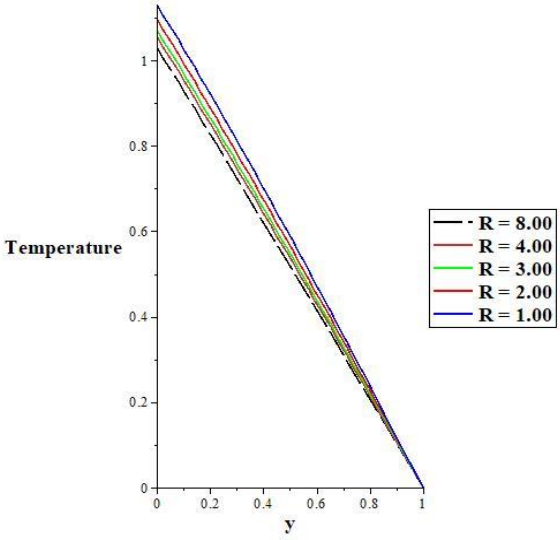

DOI: https://doi.org/10.57233/ijsgs.v11i2.853 ISSNp: 2488-9229; ISSNe: 3027-1118

Figure 10: Effect of R on the temperature.

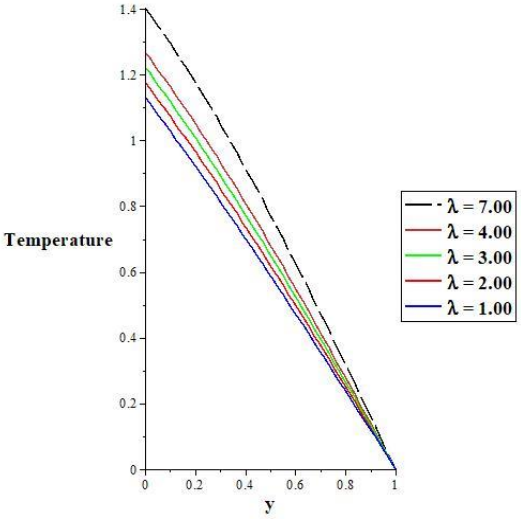

Figure 11: Effect of λ on the temperature.

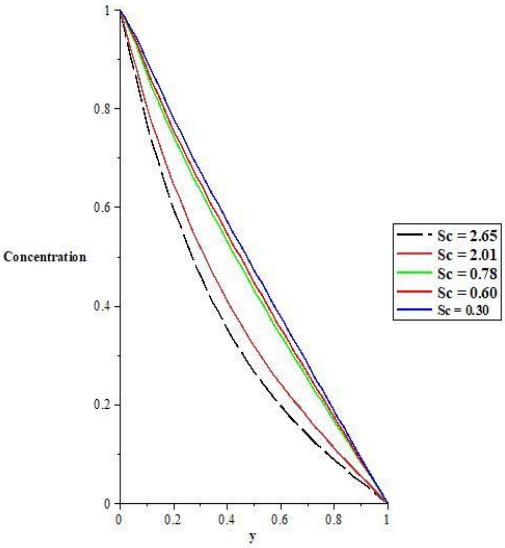

Figure 12: Effect of Sc on the concentration.

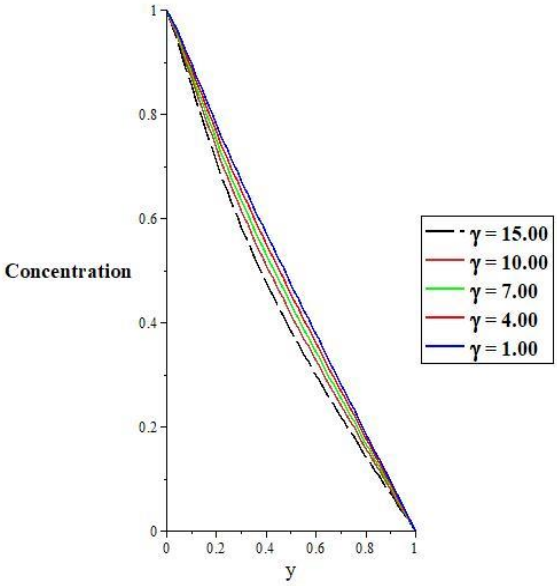

Figure 13: Effect of γ on the concentration.

5.0 CONCLUSION

Effects of heat generation and Soret on MHD Couette flow taking into account thermal radiation and mass absorption has been investigated. One of the key achievements of this research is obtaining the same results as Omokhuale and Jabaka (2022b). The major findings of this study are as follows:

i. The work of Omokhuale and Jabaka (2022b) was successfully recovered when the impact of mass absorption are neglected.
ii. Increase in heat generation leads to rise in the momentum and thermal boundary layers of the fluid. A reverse trend is seen when Prandtl number and thermal radiation become higher.
iii. Increasing the magnetic number impedes the fluid movement due to the Lorentz force action.
iv. The concentration and velocity of the fluid decreases for higher Soret and Schmidt numbers.
v. iv. The momentum boundary layer increases as both mass and thermal Grashof numbers become significant.

6.0 ACKNOWLEDGEMENT

The authors are immensely grateful for the funding received from the Tertiary Education Trust Fund (TETFund), Nigeria through Federal University Gusau, Nigeria Institutional Based Research (IBR) grant with reference number TETF/DR&D/IBR/2025VOL.I.

REFERENCES

Goud, B. S., & Reddy, Y. D. (2022). Chemical reaction and Soret effect on an unsteady MHD heat and mass transfer fluid flow along an infinite vertical plate with radiation and heat absorption. Journal of the Indian Chemical Society, 99(11). https://doi.org/10.1016/j.jics.2022.100762

Pasha, A. A., Al Mesfer, M. K., Kareem, M. W., Kodi, R., Danish, M., Patil, S., & Vaddemani, R. R. (2025). Effects of rotational forces, and thermal diffusion on unsteady magnetohydrodynamic (MHD) flow of a viscoelastic fluid through porous media with isothermal inclined plates. Case Studies in Thermal Engineering, 69. https://doi.org/10.1016/j.csite.2025.105977

Venkateswarlu, M., Lakshmi, D. V., & Makinde, O. D. (2020). Thermodynamic analysis of Hall current and Soret number effect on hydromagnetic Couette flow in a rotating system with a convective boundary condition. Heat Transfer Research, 51(1). https://doi.org/10.1615/HeatTransRes.2019027139

Sengupta, S., & Ahmed, N. (2017). MHD free convective mass transfer flow of radiative uniform heat generation (absorption) fluid through a wavy permeable channel in the presence of Soret and Dufour effects. Canadian Journal of Physics, 95(1), 44-58. https://doi.org/10.1139/cjp-2014-0599

Sengupta, S. (2015). Influences of Soret effect and thermal radiation on MHD mixed convective mass transfer flow with chemical reaction and heat generation/absorption. Communications on Applied Electronics, 1(7), 14-19. https://doi.org/10.5120/cae-1587

Bafakeeh, O. T., Raghunath, K., Ali, F., Khalid, M., Tag-ElDin, E. S. M., Oreijah, M., ... & Khan, M. I. (2022). Hall current and Soret effects on unsteady MHD rotating flow of second-grade fluid through porous media under the influences of thermal radiation and chemical reactions. Catalysts, 12(10). https://doi.org/10.3390/catal12101233

Pandey, P., & Kavitha, S. S. (2025). Chemical reaction and heat source effects on oscillatory suction in MHD flow through permeable media with Soret effect. Aircraft Engineering and Aerospace Technology, 97(2), 149-161. https://doi.org/10.1108/AEAT-01-2024-0023

Uma, M., Dinesh, P. A., & Reddy, A. S. (2019). Effects of radiation absorption, Soret and Dufour on Couette flow in an irregular channel for dusty viscoelastic fluid. Int J Sci Technol Eng Manag-A VTU Publication, 1(4), 24-30.

Ahmed, L. O., Falodun, B. O., & Abdulwaheed, J. (2020). Mechanism of Soret-Dufour, magnetohydrodynamics, heat and mass transfer flow with buoyancy force, and viscous dissipation effects. Heat Transfer, 49(5), 2831-2848. https://doi.org/10.1002/htj.21748

Kabir, T. M., Umar, A. M., & Umar, L. (2023). Magnetohydrodynamics Free Convection Couette Flow and Heat Transfer Through a Vertical Porous Plate with Heat Generation and Absorption Effect. Dutse Journal of Pure and Applied Sciences (DUJOPAS), 9, 133-145. https://dx.doi.org/10.4314/dujopas.v9i2a.13

Mat Noor, N. A., Shafie, S., Hamed, Y. S., & Admon, M. A. (2022). Soret and Dufour effects on MHD squeezing flow of Jeffrey fluid in horizontal channel with thermal radiation. Plos one, 17(5). https://doi.org/10.1371/journal.pone.0266494

Mishra, M., & Panda, J. P. (2022). Soret effect for unsteady MHD mixed convective flow in porous medium with viscous dissipation. International Journal of Ambient Energy, 43(1), 5605-5615.

Omokhuale, E., Altine, M. M. & Yusuf, A. (2019). Unsteady Heat and Mass Transfer Magnetohydrodynamic (MHD) Convective Couette Flow with Thermal Radiation using Finite Element Method (FEM). (2019). CaJoST, 1(1), 61-70. https://doi.org/10.4314/cajost.v1i1.16

Omokhuale, E., & Jabaka, M. L. (2022a). Unsteady convective couette flow with heat sink and radiation effects. FUDMA Journal of Sciences, 6(1), 266 - 277. https://doi.org/10.33003/fjs-2022-0601-873

Omokhuale E., & Lawali Jabaka, M. (2022b). Unsteady Convective Couette Flow with Heat Source. International Journal of Science for Global Sustainability, 8(1), 13. https://doi.org/10.57233/ijsgs.v8i1.317